

Tracing the Iceland plume and North East Atlantic breakup in the lithosphere

María Laura Gómez Dacal ¹, Magdalena Scheck-Wenderoth^{2,3}, Jan Inge Faleide ⁴,
Mohamed Mansour Abdelmalak ⁴, Judith Bott ²✉ & Denis Anikiev ²

Plumes are domains where hotter material rises through Earth's mantle, heating also the moving lithospheric plates that may experience thinning or even continental breakup. In particular, the Iceland plume in the NE Atlantic (NEA) could have been instrumental in facilitating the breakup between Europe and Laurentia in the earliest Eocene. Here we present an open access three-dimensional density model of the NEA crust and uppermost mantle that is consistent with previously un-integrated available data. We propose that high-density anomalies in the crust represent the preserved modifications of the lithosphere in consequence of the plate's journey over the hot mantle plume. Besides, low-density anomalies in the uppermost mantle would represent the present-day effect of the mantle plume and its interaction with the mid-ocean ridges. Overall, the model indicates that the presence of the plume together with the pre-existing crustal configuration controlled the timing, mechanisms and localization of the NEA breakup.

¹National University of La Plata, Faculty of Astronomical and Geophysical Sciences. Paseo del Bosque, B1900FWA La Plata, Argentina. ²Helmholtz Centre Potsdam-GFZ German Research Centre for Geosciences. Telegrafenberg, 14473 Potsdam, Germany. ³RWTH Aachen, Faculty of Georesources and Materials Engineering, Lochnerstr. 4-20, 52056 Aachen, Germany. ⁴Department of Geosciences, University of Oslo, Sem Sælands vei 2A, Blindern, N-0371 Oslo, Norway. ✉email: judith.bott@gfz-potsdam.de

Agreement has been reached recently that mechanisms behind continental breakup and passive margin formation encompass a continuum between mantle-driven/magma-rich and plate-driven/magma-poor deformation^{1–5}. Three-dimensional thermo-dynamic modelling studies considering magmatism^{1,2} demonstrated that mantle plumes can support continental breakup considerably if the plume meets a plate under orthogonal extension and that this can lead to the formation of magma-rich continental margins. On the other hand, dynamic three-dimensional modelling studies^{3,4} have also demonstrated that plate-driven lithospheric breakup in the absence of magma is more difficult in orthogonal extension than with some degree of obliquity. In such magma-poor settings, deformation is accommodated in simple shear leading even to mantle exhumation at the oceanic side of large-offset listric faults. In both end-member settings, variations in thickness, architecture and rheology of the lithosphere are of key importance for the breakup dynamics.

In the NE Atlantic (NEA), the successful breakup between Greenland and Eurasia at about 55 Ma was preceded by a long history of near-orthogonal (to the main structures) extensional deformation. The extensional setting, present from late Paleozoic times onward, created deep sedimentary basins but did not succeed in breaking the plates apart. Accordingly, the domains composing the present-day passive continental margins of the NEA host up to 12 km thick Cretaceous to Paleocene sedimentary units and an additional several km of pre-Cretaceous deposits^{6–8}. However, the orientation of the breakup axis is oblique to the pre-existing Paleozoic/Mesozoic rift structures of the NEA and resulted in voluminous extrusive and intrusive igneous activities^{9,10}.

In the course of this extensional history, both breakup end-members seem to have played a role and a magma-rich setting is characterizing the central part of the system at the latitude of Iceland that transitions to a less magmatic setting to the north and south. The weakening influence of a hot mantle plume is one explanation suggested for why breakup eventually succeeded. This hypothesis is also supported by reconstructions of paleo plate configurations^{11–13} and a generally thinner lithosphere beneath central Greenland interpreted as resulting from westward movement of Greenland over a thermal mantle plume^{14–16}. Contrasting models suggest (i) inherited crustal weaknesses, (ii) locally high mantle fertility or (iii) rifting-induced mantle delamination in combination with regional plate motions and stress field changes as causes of the NEA breakup (e.g.^{5,17,18}). All of these hypotheses explain the excess of magmatism and the opening of the NEA without the presence of the Icelandic mantle plume, feeding the continuous debate about its existence. Besides the discussion about the existence and type of the Iceland plume, other remaining questions concern the role it would have played in facilitating continental breakup between Eurasia and Greenland/North America, and which traces of these processes can be detected in the present-day configuration of the crust and mantle in the region. Other major focuses of disputes are the nature of the crust composing present-day Greenland-Iceland-Faroe Ridge (GIFR; e.g.¹⁹), the nature and origin of high-velocity/high-density bodies in the lower crust of the conjugate passive continental margins^{20,21} and the nature and origin of the locally thickened crust along an E-W trending domain on both sides of Iceland (GIFR), also characterized by high seismic velocities^{22,23}. In addition, there are several lines of disagreement related to the causes behind the breakup along a line cutting diagonally domains of previous crustal thinning (e.g.^{7,10}).

Though the amount of geoscientific observations has increased steadily over the past decades, integration into one consistent model representation is still lacking. With this work, we present a

three-dimensional density model of the NEA (including the conjugate continental margins of Greenland and Norway, as well as the sheared margins of the northernmost NEA, location in Fig. 1) that resolves the major structural characteristics of the crust and uppermost mantle based on the integration of multi-disciplinary geological and geophysical observations - seismic profiles, depth and thickness maps, existing models (e.g., structural geological, density; for details see Supplementary Information (SI); chapter 2), seismic mantle tomography (see SI chapter 4), and forward and inverse gravity modelling (see Methods and SI chapters 3–6). We, moreover, discuss how the model contributes to the ongoing debates in this geodynamically complex area.

Results

The three-dimensional lithospheric configuration (Fig. 2) of the presented model illustrates four main characteristics: (1) lithosphere thickness varies between less than 50 km in the oceanic and more than 250 km in the continental regions (Fig. 2j); (2) the crust is thickest (>35 km; Fig. 2e) below the continental domains and along the GIFR as imaged by the variations in Moho depth (Fig. 2c), (3) the crust encompasses thick successions (up to 21 km) of sediments (Fig. 2d) underlain by a two-layered crystalline crust (Fig. 2f, g); (4) presence of high-density/high-velocity lower crustal bodies (Fig. 2i) along the continent-ocean transition (COT), particularly in the central part of the NEA, and along the GIFR. More details about the final model are found in the Supplementary Information (SI) chapter 7, which also includes information about the data constraints (SI chapter 2) and complementary model figures.

The continental crystalline crust consists of an upper unit, characterized by lower average velocities and densities, interpreted as an indication of a felsic composition and a lower unit, characterized by higher seismic velocities and densities, interpreted as mafic. Both the upper felsic crust and the lower mafic crust, individually, have a thickness ranging between ~10 km and 40 km (Fig. 2f, g). They are thickest below the onshore parts of the continental margins and thin out considerably below the regions where crustal thinning is most severe towards the continent ocean boundary or along the Cretaceous basins. Oceanward, the COT is characterized by the occurrence of high-velocity/high-density lower crustal bodies (COT-LCBs) interpreted as a complex mixture of pre- to syn-breakup mafic and ultramafic rocks and old metamorphic rocks (e.g.^{20,21}). Laterally, the COT-LCBs merge with the lowermost layer of the oceanic crust (layer 3) contributing to a thicker than normal oceanic crust, in particular in the area of GIFR (GIFR layer 3; Fig. 2i).

Over most of the oceanic domains, the average density distribution of the crystalline crust (Fig. 3a) is uniform (2900 kg m^{-3}), apart from the regions where high-velocity/high-density bodies are present. Particularly, the higher-than-normal density area of the GIFR correlates spatially with a thicker-than-normal oceanic crust (Fig. 2h, i). In the continental domains, the average crustal density varies between 2700 kg m^{-3} and 3050 kg m^{-3} , depending on the modelled local proportion of upper and lower crust (see Methods and SI) and on the presence of high-density COT-LCBs (Fig. 2f, g, i). Accordingly, higher average densities of the crystalline crust are found below the continental margins where the COT-LCBs and a very thin continental crystalline crust are present and below the Barents Sea, a region also characterized by thinner crystalline crust²⁴ (Figs. 3a, 2e). In contrast, the average crustal density is far lower below the largest parts of onshore Greenland than below the Barents Sea and below onshore Norway. The average density of the continental domain is lower west of the Atlantic than to the east suggesting that the

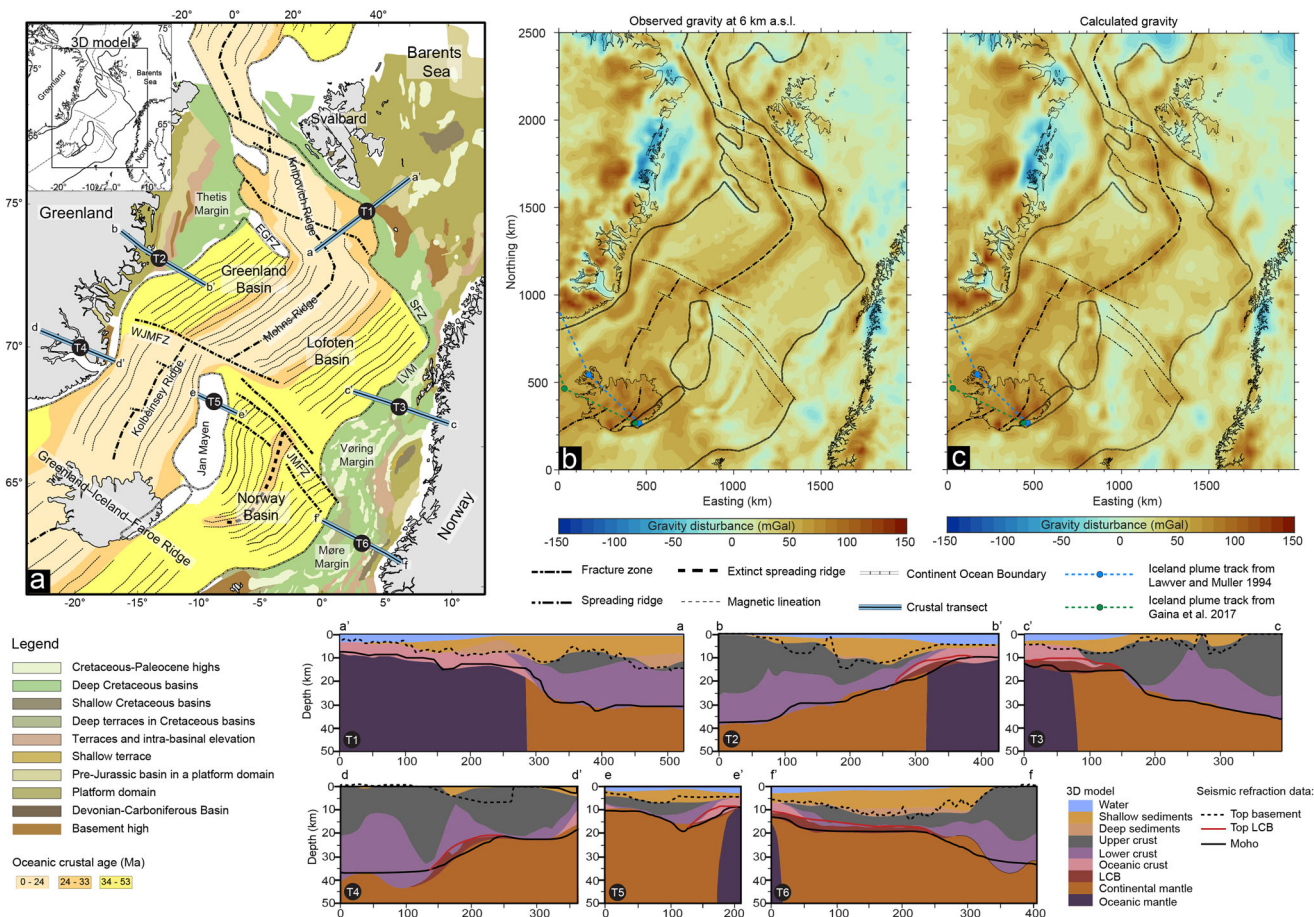


Fig. 1 Model area and examples of constraining data and model fitting. **a** Simplified structural map of the modelled area. The location of the 3D model is shown on the upper left corner. Black and blue lines mark the locations of the crustal transects (bottom of the figure), denoted as T1-6. Transects illustrate the spatial variations in the structural configuration across the 3D model with colour-coded model units and their consistency with input deep seismic refraction data (black and red lines; LCB: Lower Crustal Bodies)⁹, EGFZ: East Greenland Fault Zone, SFZ: Senja Fracture Zone, LVM: Lofoten-Vesteraleen Margin, JMFZ: Jan Mayen Fracture Zone, WJMFZ: West Jan Mayen Fracture Zone; note that the “Moho” (black line) directly refers to the image of the respective refraction seismic profile, while the “base of the crust” in the colour-coded background corresponds to the final 3D model with spatially variable constraints (“base of continental crust”, “base of oceanic crust”, “base of LCBs”) jointly integrated by means of the 3D gravity modelling procedure (detailed in the Supplementary Information, chapters 2-6). **b** Free-air gravity disturbance over the NE Atlantic region at 6 km height above sea level from EIGEN-6C4^{63,64}. **c** Calculated gravity response of the model at 6 km above sea level. The gravity response of the 3D model as a whole generally fits the observed gravity very well. The larger misfits are of high frequency, indicating some features of the area that the model is not able to resolve according to its structural resolution. Further information on all considered input data as well as explanations of remaining gravity residuals and their relation to model limitations are presented in the Supplementary Information (SI).

Greenland-American lithosphere had different properties compared to the Eurasian lithosphere and that the breakup may have occurred where a corresponding contrast in mechanical properties was present. This contrast is more pronounced in the northern part of the model, in the sheared margin domain (between northern offshore Greenland and the Barents Sea), coinciding with the area where the break-up-related magmatism is less abundant²⁵. More details on the crustal density distribution are found in the SI chapter 7.

The first-order characteristics of the mantle configuration have been obtained by converting the mantle shear wave velocities²⁶ to densities (using a Gibbs-free energy minimization approach previously described²⁷, see Methods and SI chapter 4). The derived densities were used to calculate the average mantle density distribution (Fig. 3b) that illustrates a long-wavelength variation between the oceanic domain, with generally lower mantle average densities, and the continental domain with higher average densities of the mantle. Lower-than-average mantle densities in response to higher-than-average mantle temperatures

characterize a wide region below the mid oceanic ridge (MOR), including Iceland (Fig. 3b). These low-density areas in the mantle coincide with an elevated Moho below the MOR (Fig. 2c). Only below Iceland and its surroundings (GIFR), where the oceanic crust is thicker than normal, the mantle is, nevertheless, of lower density. The lowest average density is located below the Kolbeinsey Ridge, stretching from Iceland towards the north. In contrast, the highest mantle densities in the oceanic domain correspond to the oldest oceanic areas offshore NE Greenland and offshore mid-Norway (Fig. 3b) where the base of the oceanic lithosphere also tends to be largest (Fig. 2j). The highest average mantle densities of the model area are calculated for continental domains, in particular, the larger parts below NE Greenland, the eastern Barents Sea and onshore Norway.

In the central portion of the NEA (Fig. 1a), seismological evidence^{14,26,28} reveals a low shear wave velocity anomaly indicative for higher-than-average temperatures in the uppermost mantle (as reflected also by the shallowest 1300°C-isotherm; Fig. 2j). This observation, together with the elevated topography

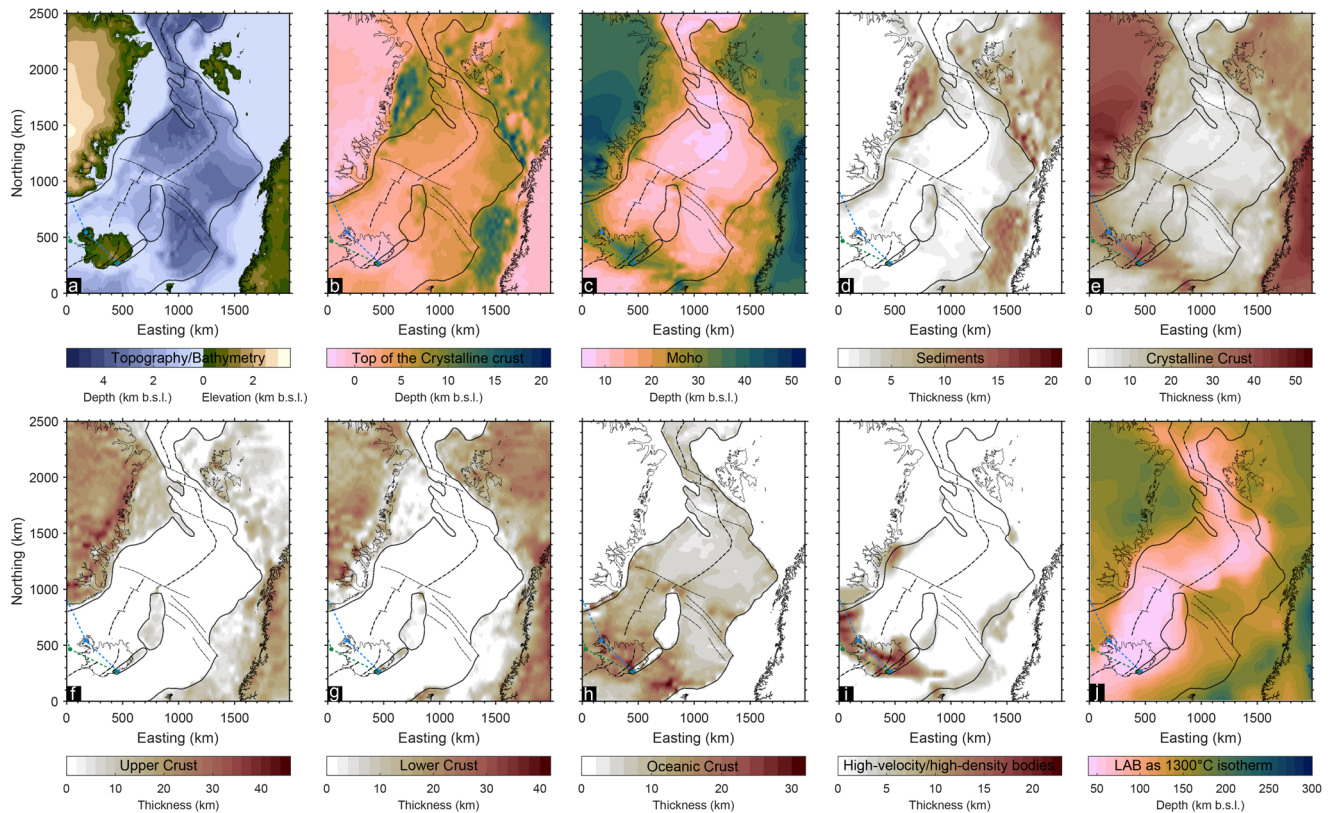


Fig. 2 Major structural characteristics of the 3D model. Upper panel: surfaces and thicknesses compiled from different data sources; lower panel: structures derived by forward and inverse gravity modelling (f-i) or the conversion of tomographic data (j). More illustrations, details and references on data sources and integration methods provided in Methods and the SI, chapter 2 and 4. **a** Topography of the elevated areas, including the ice surface in glacial areas (Greenland) and bathymetry in the ocean (ETOPO1⁶⁵). **b** Depth to the top of the crystalline basement. **c** Depth to Moho. **d** Thickness of the sedimentary layer. **e** Thickness of the crystalline crust. **f** Thickness of the upper felsic crystalline continental crust characterized by average velocities of -5.8 km s^{-1} to -6.5 km s^{-1} and an average density of 2700 kg m^{-3} . **g** Thickness of the lower mafic crystalline continental crust characterized by average velocities of -6.5 to 7 km s^{-1} and an average density of 3000 kg m^{-3} . **h** Thickness of the oceanic crust with an average density of 2900 kg m^{-3} . **i** Thickness of the lower crustal high-velocity/high-density bodies, characterized by average velocities $>7 \text{ km s}^{-1}$ and an average density of 3000 kg m^{-3} at the passive continental margins near the COT (COT-LCB; derived from ref. 21) and by an average density of 3100 kg m^{-3} along the GIRF (GIRF layer 3) as derived by forward gravity modelling. **j** Depth to the thermal Lithosphere-Asthenosphere Boundary (LAB) extracted as the 1300°C isotherm from the temperature distribution obtained by velocity conversion²⁷ of the shear wave tomography²⁶. Green and blue stippled lines are the previously proposed tracks of the Iceland plume^{39,40}.

of Iceland compared to other parts of the Mid Atlantic Ridge (Fig. 2a), were the main arguments for assuming a mantle plume beneath Iceland^{28–30}. Analyzing the mantle-velocity-derived densities in detail reveals that the mantle down to a depth of 50 km is lightest beneath Iceland (as defined for a particular depth level by the first percentile of the lowest densities; Fig. 4). Below this level, between 50 and 100 km depth, the domain of the low-density anomaly extends north to also include the region below the Kolbeinsey Ridge, west of the Jan Mayen microcontinent (Fig. 4). Moving downwards, below 100 km depth, the anomaly locates only beneath the Kolbeinsey Ridge, whereas the density decrease is less pronounced below Iceland. Thus, a continuous low-density body from the shallow interval to larger depths can be traced only north of Iceland and connects the shallow Iceland anomaly to the one beneath the mid ocean Kolbeinsey Ridge. Accordingly, Iceland itself is located above a southward protrusion of the density anomaly rising continuously vertically along the Kolbeinsey Ridge from more than 200 km depth (Fig. 4a).

Only the mantle configuration in the central part of the NEA, delineated by magma-rich passive rifted margins on either side (high-density bodies; Fig. 2i) is dominated by low densities (Figs. 3b, 4a), whereas less magmatic margin segments with overall higher mantle density prevail towards the south and

north. Particularly, the 3D density model illustrates the correlation between the denser (and thus colder) mantle and the less magmatic setting at the northern NEA margins, also coinciding with a change in the opening regime from an orthogonal passive margin in the central part to a sheared margin in the north (Figs. 1, 4). The only low-density/low-velocity anomaly in the northern NEA is a smaller-scale feature observed from 140 km to 220 km depth north of the Knipovich Ridge (Fig. 4; see SI chapter 4) that can be related to higher mantle temperatures under the MOR.

Modelling a large volume as the entire NEA lithosphere while resolving details as small as some sub-basin sediment thicknesses inevitably involves large observational gaps (detailed input data explanation is found in SI chapter 2) and thus uncertainties. Besides, the integration of a large number of different datasets, with their individual uncertainties, derives in a comparatively large uncertainty. In this case, the confidence in the model strongly depends on a convincing data integration process (SI chapters 2–6). In order to provide transparency with regard to the modelling procedure and an idea of the robustness of the main results of the model, we show the stepwise procedure and residuals derived by each modelling decision in the SI (chapters 2–6). We regard this model as a reasonable and useful one due to the

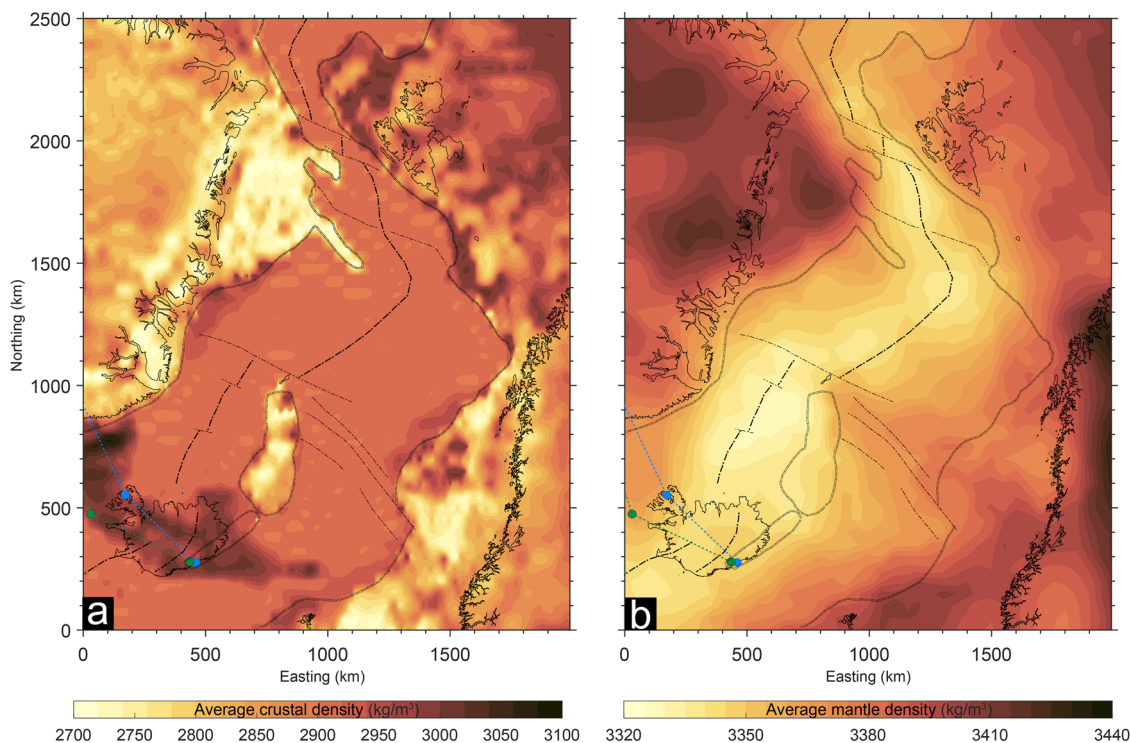


Fig. 3 First-order density configuration of the model. **a** average density of the crystalline crust. **b** Average density of the upper mantle between the Moho and 300 km depth. Green and blue stippled lines are the proposed tracks of the Iceland plume obtained from two different sources^{39,40}. More details and figures of the mantle density distribution can be found in the SI, chapter 4.

increased knowledge it provides compared to the unrelated information of all the individual input datasets. Besides, the results and main outcomes of the 3D model (see Discussion) are robust and do not change considerably to variations of the main sources of error.

Discussion

The present-day three-dimensional density configuration of the crust and upper mantle in the NEA reveals the past traces left by the breakup of a continental plate in response to extension and plume-lithosphere interactions, as we can see from its relation to various other observations. On both sides of the NEA, the normal-faulted passive continental margins prove that extensional stresses have influenced the breakup process. That several extensional phases in the Mesozoic did not succeed in continental breakup has been explained by different mechanisms^{8,10,31–33}. Among others, discussed reasons for unsuccessful breakup before the Eocene include: (i) insufficiently large extension to break a thick and strong lithosphere; (ii) strain hardening of the rifted domains in response to the rifting velocity being slower than conductive cooling of the rifting-related thermal anomaly; (iii) cessation of extensional forcing before breakup; or (iv) non-optimal alignment of stress-directions and orientation of pre-existing fabrics and weaknesses. The fact that rifting was successful in the earliest Eocene, in spite of rather minor extension, could be explained as being due to additional support by a thermal anomaly in the mantle³⁴. Such dynamic support by a buoyant hot mantle would also be consistent with the presence of an erosional breakup unconformity on both passive margins. The unconformity documents that these domains have been uplifted shortly before or syn-breakup, right after a phase of deep marine conditions in the late Cretaceous-early Paleocene³⁵. Finally, the presence of large volumes of magmatic products near the COT of the central NEA (Fig. 2i) indicates that the breaking lithosphere

was hot. Such magmatic products are documented in the deeper crust as COT-LCBs (Fig. 2i), as sill intrusions in the sedimentary basins and as extrusive volcanics, including basaltic flows penetrated by several boreholes offshore Norway³⁶. The amount of magmatism per se is difficult to explain without a plume³⁷. Besides, the associated elevated mantle temperatures/low densities (Figs. 3b, 4), as well as the shallower than normal NEA bathymetry (Fig. 2a) compared to a plate cooling model³⁸, both can be explained by the activity of a mantle plume. That the crust is both thicker (Fig. 2e; see also³⁷) and denser than normal (Fig. 3a) in the oceanic area along the GIFR and that this region coincides spatially with the proposed tracks of the Iceland plume reconstructed by independent methods^{39,40} is the cherry on the cake of our findings. It is this latter finding that strongly supports the arrival of the mantle plume and its subsequent track in the moving plates above.

The contrasting hypothesis that the Icelandic crust is continental¹⁹ is not supported by our model. To achieve consistency with observed gravity (Fig. 1b) while considering crustal thicknesses as indicated by active seismic profiles, rather high average crustal densities in the region of Iceland are required that are far higher than typical continental crustal densities (Fig. 3a). As seismic tomography (i.e., different independent models as shown in SI chapter 4.4) demonstrates that the GIFR area and larger surroundings are characterized by low mantle densities (Fig. 3b), the upper mantle cannot balance the mass deficit either. Therefore, the contribution to the required gravity response has to come from the crust. We cannot exclude, however, that continental blocks may be baked into the mélange of magmatic products formed during the breakup process¹², in particular when associated with rift jumps^{41,42}.

Another interesting finding is a general difference in average density of the crust for the continental domain of Norway compared to the one of Greenland, at margins that are corresponding conjugates (Fig. 3a). To the north of the magma-rich

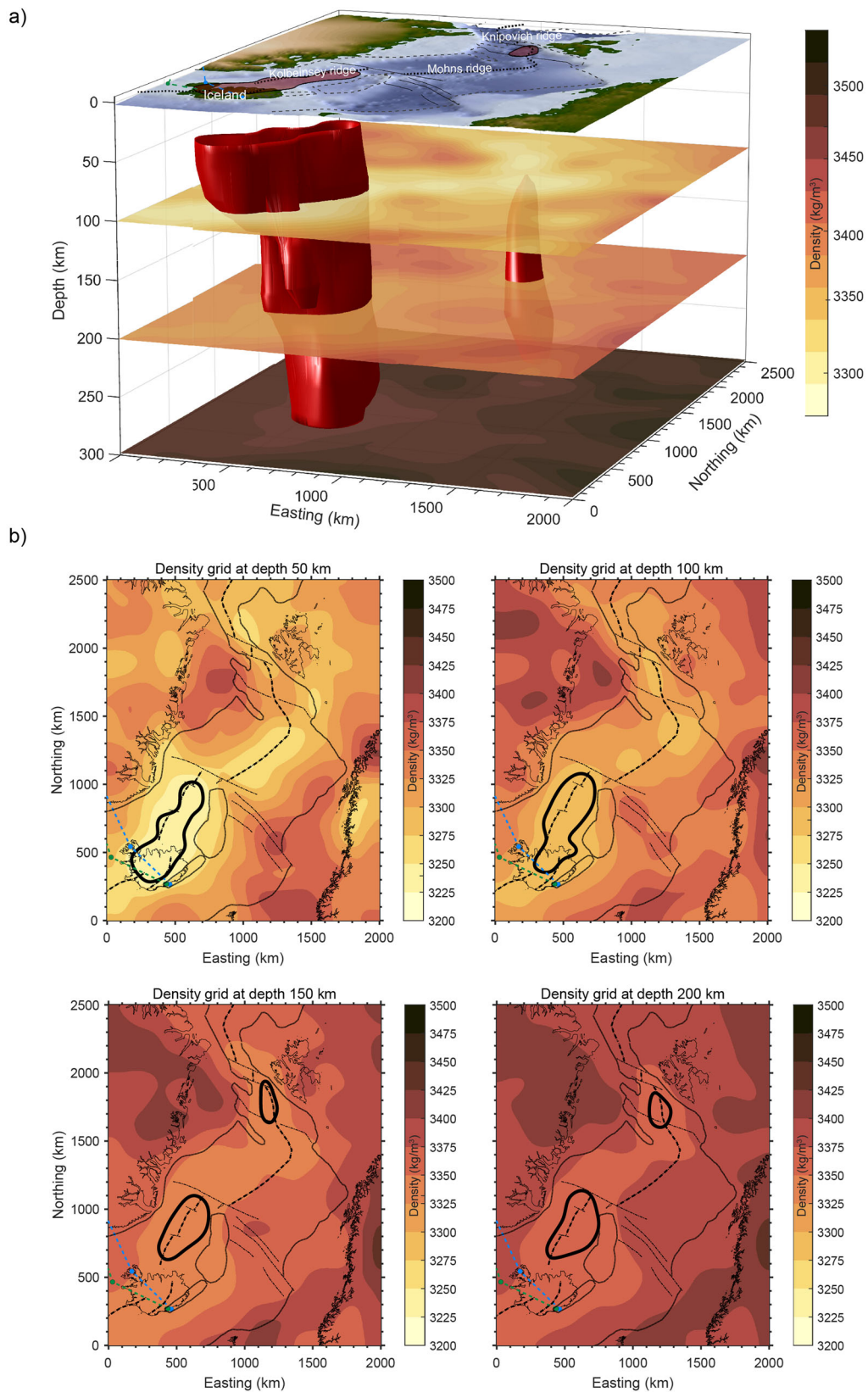


Fig. 4 Detailed mantle density structure. **a** 3D image of a low-density body in the mantle statistically delimited by the 1st percentile of the lowest densities at each depth. **b** Depth slices of density distribution at 50 km depth intervals. The black curves show the location of the 1st percentile of lowest densities at each depth.

central NEA margin (north of the EGFZ, Fig. 1), a change in regime is observed switching to a less magmatic sheared margin. The model indicates that the crust also contains less high-velocity/high-density bodies in this area where also the highest contrast of crustal average density between both corresponding conjugate margins (Fig. 3a) is detected. Considering the larger distance of the sheared margin to the plume, the latter was less influential in this region and accordingly less magmatic products are observed. This suggests that the localization of the rupture may have been guided by an ancient difference in rheology between the two plates for which the modelled large contrast in average crustal density could be an indication. These characteristics may have defined the opening regime of oblique extension as a preferred mechanism in a plate-driven breakup setting^{3,4}.

The mantle velocity-temperature-density configuration additionally correlates spatially with features observed at present-day in the area: regions of high temperature and low density correlate with the current plume position (as derived from different studies^{39,40}) and the MOR, especially to the north of Iceland (Kolbeinsey Ridge). Particularly, the lower than normal average densities of the model are arranged in a body that is located below the centre of Iceland at shallow depths, coinciding with the track of the plume of the last 20 Ma (Fig. 4). However, its continuation in depth is found beneath the Kolbeinsey Ridge (see also^{28,43}). The spatial correlation between the low-velocity body, Iceland and the MOR to its north could lead to different interpretations. Considering that the shape of the body differs from the expected vertically continuous conduit-type shape of a plume, the anomaly could be an expression of the interaction of the plume with the MOR (see also⁴⁴) changing abruptly along the Jan Mayen Fracture Zone^{45,46}. The low-density zone extended in depth only below the Kolbeinsey Ridge could be interpreted as a stronger influence of the MOR compared to the plume. The interrogation about the present-day activity of the plume remains open to interpretations with the model results. As two end-member concepts, the low-density body could be interpreted, on the one hand, as a non-vertically continuous plume or, on the other, as a relic of a vanished plume remaining only an anomalously hot MOR. Several tomography models, (e.g.^{44,47}) coincide in the observation of low velocity anomalies that are related to two or more separate hotspots located along the MOR between the Reykjanes Ridge and the northern Kolbeinsey Ridge though the breadth of the inferred hot anomaly may vary between models. Common to most of the existing tomography models, however, is that distinct anomalies at shallowest mantle depths tend to merge into a single low-velocity anomaly at larger upper mantle depths.

Previous works attempted to characterize the lithospheric density (or temperature) distribution of the North Atlantic area (e.g.^{48–50}). All of them used different methodologies, input data, defined different working areas and, mainly, pursued a different aim than the study presented here. Gravity field interpretations were done before^{48,49}, but for a broader area, with very different input data and aiming specifically to characterize either the crust or the upper mantle, respectively, and not both. Yet another study⁵⁰ pursued a very different objective, namely to obtain the horizontal stresses by modelling the density distribution as a previous step. The general conclusions of the mentioned works do not contradict our main findings. Specially, all of them mentioned anomalous characteristics in Iceland and its surroundings (higher density within the crust, thermally related low density in the upper mantle, anomalous mantle pressure related to melt) that are coincident with our conclusions.

In summary, the geophysical lithospheric configuration of the NEA, derived from various observations, demonstrates that the continental and oceanic crust preserved different aspects of the NEA history including several phases of extension, the thermal

and magmatic imprints of the arriving mantle plume during and after the plate breakup and the subsequent cooling. The crust also preserved the changes in opening regime in response to the increasing distance to the plume, expressed as a transition between a magma-rich margin formation close to the plume and a less magmatic sheared margin setting at larger distance from the plume. In contrast, the upper mantle structure images the geodynamic processes active today, and their interactions: vertically continuous domains of lower densities and higher temperatures below the present-day MOR and shallow mantle levels below Iceland point to a less important role of the plume today as compared to an increasingly stronger influence of the MOR anomaly.

Methods

Apart from the integration of structural characteristics derived from seismic and seismological imaging of the crust and mantle, diverse data compilations and previously built structural models, we additionally constrained the density distribution by three-dimensional gravity modelling. Gravity modelling was applied by forward calculating the gravity response of a certain density configuration using IGMAS +^{51,52} and complemented by inverting the residuals found between observed and calculated gravity (Fatiando a Terra^{53,54}). Details concerning all the integrated data and the modelling methodology are given in the SI (chapter 2 and chapters 3–6, respectively).

The major interfaces compiled from seismic data and previous models and compilations are the top to the crystalline crust, the top of the high-velocity/high-density bodies located in the surroundings of the COT (COT-LCBs) and the crust-mantle boundary (Moho) (Fig. 2b, c, i, respectively), as well as, the topography, bathymetry and the base of the ice (Fig. 2a). The thickness of the sedimentary deposits (Fig. 2d) was compiled from different sources (main source GlobSed v3⁵⁵, replaced by local higher resolution information in some regions^{6,8,24,56}) detailed in SI, chapter 2. The thickness of the COT-LCBs unit was obtained from the compilation of ref. ²¹ who interpreted a large seismic database from different sources. The depth to the Moho was compiled from several deep seismic data sets, receiver function studies and previously published compilations and models^{24,57–60} (see more details in SI, chapter 2). To differentiate oceanic and continental domains, the continent ocean boundary compiled by Abdelmalak et al.²¹ was considered.

In the first step, the units derived from data compilation were integrated into an initial 3D model with 7 layers, from top to bottom: water, ice, uniform sediments, uniform continental crust, uniform oceanic crust, COT-LCBs and uniform mantle. The scattered data describing the top surface elevation of the units were interpolated to obtain regular grids with a horizontal element spacing of 10 km (Convergent Interpolation algorithm of Petrel, ©Schlumberger, 2011.1.2). Further differentiation of the model in terms of spatial variations in crustal and mantle densities relied on additional deep seismic data sets. These contained depth information for major interfaces and seismic velocities that could be converted to densities. Within an iterative workflow of forward and inverse gravity modelling, we closed the gaps between the deep seismic information for which the velocity-derived densities were kept fixed. Thus, we sequentially refined the model always comparing it with the observed free-air gravity disturbances (EIGEN-6C4 at 6 km depth; Fig. 1b; more details in SI, chapters 3–6) following a stepwise procedure:

- (1) Shear wave velocities of a tomographic model (an update of the Collaborative Seismic Earth Model “CSEM Europe”, 2nd generation²⁶) were converted to temperatures and densities, using the Gibbs free-energy minimization

method^{61,62} as implemented in a Python application developed for an earlier study²⁷. A detailed description of the tomographic model and the conversion method, including assumptions and parameters involved, is presented as SI (chapter 4).

- (2) To account for compaction-driven density increase with depth, the sedimentary unit was divided into a shallow and a deep part (as detailed in the SI, chapter 5). The shallow portion above 8 km depth (below sea level) is considered as still possessing a degree of porosity and thus a lower average density. Below 8 km depth, sediments are considered sufficiently compacted to have a higher average density.
- (3) In the oceanic domain, several seismic profiles of the Greenland-Iceland-Faroe Ridge (GIFR) area image a thicker than normal layer 3 that additionally coincides with a positive gravity residual. Therefore, we modelled the geometry of a high-velocity/ high-density body (GIFR layer 3) by fitting the observed gravity but preserving the constraints given by the seismic information where they are available.
- (4) The remaining gravity residuals in continental areas were inverted for crustal density variations. Deep refraction velocities along existing seismic profiles indicate that the continental crystalline crust is composed of an upper felsic and a lower mafic unit. The respective P-wave velocities were converted to average densities of the respective crustal interval and the interface between the felsic and the mafic continental crust was determined by inversion of the gravity residuals using a modified version of the Harvester module⁵⁴ of Fatiando a Terra⁵³.

Data availability

The global gravity field model “EIGEN-6C4”^{24,25} is freely available from the International Centre for Global Earth Models (ICGEM) website (<http://icgem.gfz-potsdam.de>), where also the specific components used for this study can be calculated (<http://icgem.gfz-potsdam.de/calgrid>) and retrieved. The input mantle tomography data (“CSEM Europe”, 2nd generation²⁷) are available together with the final gravity modelling results of this publication through the GFZ Data Services repository under the <https://doi.org/10.5880/GFZ.4.5.2023.001>. This repository includes (i) a grid of input vertical and horizontal shear-wave velocity values for the mantle part of the model, complemented by the corresponding density values obtained through conversion as well as (ii) information on the geometries (depth and thickness distributions) and densities of the crustal model units.

Code availability

Shear wave velocities were converted to densities with the open-source Python application “V2RhoT_gibbs” (<https://doi.org/10.5281/zenodo.6538257>). The 3D gravity modelling was carried out using the freely available (no-cost license) software “IGMAS+” (<https://doi.org/10.5880/GFZ.4.5.IGMAS.V.1.3>, <https://www.gfz-potsdam.de/igmas>) and modules of the open-source code “Fatiando a Terra” (<https://legacy.fatiando.org>). The integration of original structural data and the creation of gridded interfaces was performed with the commercial software “Petrel” (©Copyright Schlumberger). Geographic coordinate conversions were done with GMT Version 6 (©Copyright 2019 - 2023, The GMT Developers; Wessel et al. (2019); <https://doi.org/10.1029/2019GC008515>). For the creation of maps “Golden Software Surfer”, “ArcGIS” and MATLAB® (version R2022b) have been used and we have finalized figures with “Adobe Illustrator”.

Received: 18 May 2023; Accepted: 17 November 2023;

Published online: 06 December 2023

References

1. Burov, E. & Gerya, T. Asymmetric three-dimensional topography over mantle plumes. *Nature* **513**, 85–89 (2014).
2. Koptev, A., Ehlers, T. A., Nettekheim, M. & Whipp, D. M. Response of a rheologically stratified lithosphere to subduction of an indenter-shaped plate: Insights into localized exhumation at orogen syntaxes. *Tectonics* **38**, 1908–1930 (2019).
3. Brune, S., Popov, A. A. & Sobolev, S.V. Modeling suggests that oblique extension facilitates rifting and continental break-up. *J. Geophys. Res.: Solid Earth* **117** (2012).
4. Le Pourhiet, L. et al. Continental break-up of the South China Sea stalled by far-field compression. *Nat. Geosci.* **11**, 605–609 (2018).
5. Petersen, K. D., Schiffer, C. & Nagel, T. LIP formation and protracted lower mantle upwelling induced by rifting and delamination. *Sci. Rep.* **8**, 16578 (2018).
6. Zastrozhnov, D. et al. Regional structure and polyphased Cretaceous–Paleocene rift and basin development of the mid-Norwegian volcanic passive margin. *Mar. Petroleum Geol.* **115**, 104269 (2020).
7. Gernigon, L. et al. A digital compilation of structural and magmatic elements of the Mid-Norwegian continental margin (version 1.0). *Norwegian J. Geology/ Norsk Geologisk Forening* **101** (2021).
8. Scheck-Wenderoth, M., Raum, T., Faleide, J., Mjelde, R. & Horsfield, B. The transition from the continent to the ocean: a deeper view on the Norwegian margin. *J. Geol. Soc.* **164**, 855–868 (2007).
9. Abdelmalak, M. M. et al. Quantification and restoration of the pre-drift extension across the NE Atlantic conjugate margins during the mid-Permian–early Cenozoic multi-rifting phases. *Tectonics* **42**, e2022TC007386 (2023).
10. Gernigon, L. et al. Crustal fragmentation, magmatism, and the diachronous opening of the Norwegian–Greenland Sea. *Earth-Sci. Rev.* **206**, 102839 (2020).
11. Gaina, C., Gernigon, L. & Ball, P. Palaeocene–Recent plate boundaries in the NE Atlantic and the formation of the Jan Mayen microcontinent. *J. Geol. Soc.* **166**, 601–616 (2009).
12. Torsvik, T. H. et al. Continental crust beneath southeast Iceland. *Proc. Natl Acad. Sci. USA* **112**, E1818–E1827 (2015).
13. Steinberger, B., Bredow, E., Lebedev, S., Schaeffer, A. & Torsvik, T. H. Widespread volcanism in the Greenland–North Atlantic region explained by the Iceland plume. *Nat. Geosci.* **12**, 61–68 (2018).
14. Lebedev, S., Schaeffer, A. J., Fullea, J. & Pease, V. Seismic tomography of the Arctic region: inferences for the thermal structure and evolution of the lithosphere. *Geol. Soc. Lond. Special Publ.* **460**, 419–440 (2018).
15. Mordret, A. Uncovering the Iceland Hot Spot Track Beneath Greenland. *J. Geophys. Res.: Solid Earth* **123**, 4922–4941 (2018).
16. Toyokuni, G., Matsuno, T. & Zhao, D. P-wave tomography beneath Greenland and surrounding regions: 2. lower mantle. *J. Geophys. Res.: Solid Earth* **125**, (2020).
17. Foulger, G. R. & Anderson, D. L. A cool model for the Iceland hotspot. *J. Volcanol. Geotherm. Res.* **141**, 1–22 (2005).
18. Schiffer, C. et al. Structural inheritance in the North Atlantic. *Earth-Sci. Rev.* **206**, 102975 (2020).
19. Foulger, G. R. et al. The Iceland microcontinent and a continental Greenland–Iceland–Faroe ridge. *Earth-Sci. Rev.* **206**, 102926 (2020).
20. Gernigon, L. et al. A moderate melting model for the Vøring margin (Norway) based on structural observations and a thermo-kinematic modelling: implication for the meaning of the lower crustal bodies. *Tectonophysics* **412**, 255–278 (2006).
21. Abdelmalak, M. M. et al. The T-reflection and the deep crustal structure of the Vøring Margin, Offshore mid-Norway. *Tectonics* **36**, 2497–2523 (2017).
22. Richardson, K., Smallwood, J., White, R., Snyder, D. & Maguire, P. Crustal structure beneath the Faroe Islands and the Faroe–Iceland ridge. *Tectonophysics* **300**, 159–180 (1998).
23. Holbrook, W. S. et al. Mantle thermal structure and active upwelling during continental breakup in the North Atlantic. *Earth Planet Sci Lett* **190**, 251–266 (2001).
24. Klitzke, P., Faleide, J. I., Scheck-Wenderoth, M. & Sippel, J. A lithosphere-scale structural model of the Barents Sea and Kara Sea region. *Solid Earth* **6**, 153–172 (2015).
25. Meza-Cala, J. C., Tsikalas, F., Faleide, J. I. & Abdelmalak, M. M. New insights into the late Mesozoic–Cenozoic tectono-stratigraphic evolution of the northern Lofoten–Vesterålen margin, offshore Norway. *Mar. Petroleum Geol.* **134**, 105370 (2021).
26. Noe, S. et al. Collaborative seismic earth model: generation 2. In: AGU Fall Meeting Abstracts 2021, S15E–S10298 (2021).
27. Kumar, A., Cacace, M., Scheck-Wenderoth, M., Götze, H. J. & Kaus, B. J. P. Present-day upper-mantle architecture of the alps: insights from data-driven dynamic modeling. *Geophys. Res. Lett.* **49** (2022).
28. Rickers, F., Fichtner, A. & Trampert, J. The Iceland–Jan Mayen plume system and its impact on mantle dynamics in the North Atlantic region: Evidence from full-waveform inversion. *Earth Planet. Sci. Lett.* **367**, 39–51 (2013).
29. Wolfe, C. J., VanDecar, J. C. & Solomon, S. C. Seismic structure of the Iceland mantle plume. *Nature* **385**, 245–247 (1997).
30. Barnett-Moore, N., Hassan, R., Flament, N. & Müller, D. The deep Earth origin of the Iceland plume and its effects on regional surface uplift and subsidence. *Solid Earth* **8**, 235–254 (2017).

31. Tsikalas, F., Faleide, J. I., Eldholm, O. & Blaich, O. A. in *Regional Geology and Tectonics: Phanerozoic Passive Margins, Cratonic Basins and Global Tectonic Maps 1* (eds Roberts, D. G. & Bally, A. W.), 140–201 (Elsevier, 2012).
32. Brekke, H. The tectonic evolution of the Norwegian Sea continental margin, with emphasis on the Voring and More basins. *Special Publ.-Geol. Soc. Lond.* **167**, 327–378 (2000).
33. Van Wijk, J. & Cloetingh, S. Basin migration caused by slow lithospheric extension. *Earth Planet Sci. Lett.* **198**, 275–288 (2002).
34. Skogseid, J. et al. NE Atlantic continental rifting and volcanic margin formation. *Geol. Soc. Lond. Spec. Publ.* **167**, 295–326 (2000).
35. Dam, G., Larsen, M. & S nderholm, M. Sedimentary response to mantle plumes: Implications from Paleocene onshore successions, West and East Greenland. *Geology* **26**, 207–210 (1998).
36. Planke, S., Rasmussen, T., Rey, S. S. & Myklebust, R. in *Geological Society, London, Petroleum Geology Conference series* (eds Dor , A. G. & Vining, B. A.) 833–844 (Geological Society of London, 2005).
37. White, R. S. Rift–plume interaction in the North Atlantic. *Philos. Trans. Roy. Soc. Lond. Ser. A: Math. Phys. Eng. Sci.* **355**, 319–339 (1997).
38. Jones, S. M., White, N., Clarke, B. J., Rowley, E. & Gallagher, K. Present and past influence of the Iceland Plume on sedimentation. *Geol. Soc. Lond. Spec. Publ.* **196**, 13–25 (2002).
39. Gaina, C., Nasuti, A., Kimbell, G. S. & Blischke, A. Break-up and seafloor spreading domains in the NE Atlantic. *Geol. Soc. Lond. Spec. Publ.* **447**, 393–417 (2017).
40. Lawver, L. A. & M ller, R. D. Iceland hotspot track. *Geology* **22**, 311–314 (1994).
41. Bohnhoff, M. & Makris, J. Crustal structure of the southeastern Iceland–Faeroe Ridge (IFR) from wide aperture seismic data. *J. Geodyn.* **37**, 233–252 (2004).
42. Yuan, X., Korenaga, J., Holbrook, W. S. & Kelemen, P. B. Crustal structure of the greenland-iceland ridge from joint refraction and reflection seismic tomography. *J. Geophys. Res.: Solid Earth* **125** (2020).
43. Pilidou, S., Priestley, K., Debayle, E. & Gudmundsson,  . Rayleigh wave tomography in the North Atlantic: high resolution images of the Iceland, Azores and Eifel mantle plumes. *Lithos* **79**, 453–474 (2005).
44. Celli, N. L., Lebedev, S., Schaeffer, A. J. & Gaina, C. The tilted Iceland Plume and its effect on the North Atlantic evolution and magmatism. *Earth. Planet. Sci. Lett.* **569** (2021).
45. Koptev, A., Cloetingh, S., Burov, E., Francois, T. & Gerya, T. Long-distance impact of Iceland plume on Norway’s rifted margin. *Sci. Rep.* **7**, 10408 (2017).
46. Tan, P., Sippel, J., Breivik, A. J., Mee en, C. & Scheck-Wenderoth, M. Lithospheric control on asthenospheric flow from the Iceland plume: 3-D density modeling of the Jan Mayen–East Greenland Region, NE Atlantic. *J. Geophys. Res.: Solid Earth* **123**, 9223–9248 (2018).
47. Schaeffer, A. J. & Lebedev, S. Global shear speed structure of the upper mantle and transition zone. *Geophys. J. Int.* **194**, 417–449 (2013).
48. Haase, C. J. T. G., Ebbing, J. & Funck, T. A 3D regional crustal model of the NE Atlantic based on seismic and gravity data. *Geol. Soc. Lond. Spec. Publ.* **447**, 233–247 (2017).
49. Shulgin, A. & Artemieva, I. M. Thermochemical heterogeneity and density of continental and oceanic upper mantle in the European–North Atlantic region. *J. Geophys. Res.: Solid Earth* **124**, 9280–9312 (2019).
50. Schiffer, C. & Nielsen, S. B. Implications for anomalous mantle pressure and dynamic topography from lithospheric stress patterns in the North Atlantic Realm. *J. Geodyn.* **98**, 53–69 (2016).
51. G tze, H.-J. & Lahmeyer, B. Application of three-dimensional interactive modeling in gravity and magnetics. *Geophysics* **53**, 1096–1108 (1988).
52. Anikiev, D. et al. IGMAS+: Interactive Gravity and Magnetic Application System (Version 1.3) (GFZ Data Services, 2020).
53. Uieda, L., Oliveira Jr, V. C. & Barbosa, V. C. Modeling the earth with fatiando a terra. In: *Proc. 12th Python in Science Conference* (Walt, S. v. d., Millman, J. & Huff, K.) 96–103 (SciPy, 2013).
54. Mee en, C. *The Thermal and Rheological State of the Northern Argentinian Foreland Basins* Doctoral Dissertation, University of Potsdam (2019).
55. Straume, E. O. et al. GlobSed: Updated Total Sediment Thickness in the World’s Oceans. *Geochemistry, Geophysics, Geosystems* **20**, 1756–1772 (2019).
56. Granath, J., Whittaker, R. & Dinkelmann, M. Long offset seismic reflection data and the crustal structure of the NE Greenland Margin. In: *AGU Fall Meeting Abstracts*. T43G-T42467.
57. Funck, T. et al. Moho and basement depth in the NE Atlantic Ocean based on seismic refraction data and receiver functions. *Geol. Soc. Lond. Spec. Publ.* **447**, 207–231 (2017).
58. Petrov, O. et al. Crustal structure and tectonic model of the Arctic region. *Earth-Sci. Rev.* **154**, 29–71 (2016).
59. Maystrenko, Y. P., Bayer, U. & Scheck-Wenderoth, M. Regional-scale structural role of Permian salt within the Central European Basin System. *Geol. Soc. Lond. Spec. Publ.* **363**, 409–430 (2012).
60. Kraft, H. A., Thybo, H., Vinnik, L. P. & Oreshin, S. Crustal structure in central-eastern Greenland from receiver functions. *J. Geophys. Res.: Solid Earth* **124**, 1653–1670 (2019).
61. Connolly, J. A. D. Computation of phase equilibria by linear programming: A tool for geodynamic modeling and its application to subduction zone decarbonation. *Earth. Planet. Sci. Lett.* **236**, 524–541 (2005).
62. Connolly, J. A. D. The geodynamic equation of state: What and how. *Geochem. Geophys. Geosyst.* **10** (2009).
63. F rste, C. et al. EIGEN-6C4–The latest combined global gravity field model including GOCE data up to degree and order 1949 of GFZ Potsdam and GRGS Toulouse. *EGUGA*, 3707 (2014).
64. Ince, E. S. et al. ICGEM–15 years of successful collection and distribution of global gravitational models, associated services, and future plans. *Earth Syst. Sci. Data* **11**, 647–674 (2019).
65. Amante, C. & Eakins, B. W. ETOPO1 arc-minute global relief model: procedures, data sources and analysis. *NOAA Technical Memorandum NESDIS NGDC-24*, (2009).

Acknowledgements

M.L.G.D. was partially supported by grants from the ESM project of the Helmholtz Impulse and Networking Funds. M.M.A. was funded by the Norwegian Petroleum Directorate (NPD) and Research Centre for Arctic Petroleum Exploration (ARCEX). J.I.F. received support from the University of Oslo during his sabbatical at GFZ Potsdam. We thank Dr. Christian Mee en for his technical support during the data integration and gravity modelling procedure. Finally, we would like to thank two anonymous reviewers for their critical comments that helped to improve the originally submitted versions of the manuscript.

Author contributions

All authors together developed the research idea and evaluated the results. M.L.G.D. built the structural model, performed the gravity calculations and wrote the first version of the manuscript. M.S.W. supervised the modelling procedure and provided her proficiency in drafting the manuscript. J.I.F. contributed the expertise on the available data, most of the input data compilations and the geological history. MMA contributed with new interpretations of several seismic profiles and other available data and composed some of the Figures. JB co-supervised the data integration and gravity modelling. DA helped to handle the data and visualize the results, including the composition of some Figures. All authors contributed to the discussion and interpretation of the results, revised the manuscript and were partially responsible for obtaining the financial support to develop this research.

Funding

Open Access funding enabled and organized by Projekt DEAL.

Competing interests

The authors declare no competing interests.

Additional information

Supplementary information The online version contains supplementary material available at <https://doi.org/10.1038/s43247-023-01120-w>.

Correspondence and requests for materials should be addressed to Judith Bott.

Peer review information *Communications Earth & Environment* thanks the anonymous, reviewers for their contribution to the peer review of this work. Primary Handling Editors: Jo o Duarte and Joe Aslin. Peer reviewer reports are available.

Reprints and permission information is available at <http://www.nature.com/reprints>

Publisher’s note Springer Nature remains neutral with regard to jurisdictional claims in published maps and institutional affiliations.

 **Open Access** This article is licensed under a Creative Commons Attribution 4.0 International License, which permits use, sharing, adaptation, distribution and reproduction in any medium or format, as long as you give appropriate credit to the original author(s) and the source, provide a link to the Creative Commons licence, and indicate if changes were made. The images or other third party material in this article are included in the article’s Creative Commons licence, unless indicated otherwise in a credit line to the material. If material is not included in the article’s Creative Commons licence and your intended use is not permitted by statutory regulation or exceeds the permitted use, you will need to obtain permission directly from the copyright holder. To view a copy of this licence, visit <http://creativecommons.org/licenses/by/4.0/>.

  The Author(s) 2023